PCCP

Energy Loss Analysis in Photoelectrochemical Water Splitting: A Case Study of Hematite Photoanode

Journal:	*Physical Chemistry Chemical Physics*
Manuscript ID	CP-ART-06-2018-004021.R1
Article Type:	Paper
Date Submitted by the Author:	02-Aug-2018
Complete List of Authors:	Wang, Zhiliang; University of Queensland, Lyu, Miaoqiang; The University of Queensland, School of Chemical Engineering Chen, Peng; University of Queensland, School of Chemical Engineering and Australian Institute for Bioengineering and Nanotechnology Wang, Songcan; The University of Queensland , Chemical Engineering Wang, Lianzhou; ARC Centre of Excellence for Functional Nanomaterials, The University of Queensland

Journal Name

ARTICLE

Energy Loss Analysis in Photoelectrochemical Water Splitting: A Case Study of Hematite Photoanodes

Received 00th January 20xx,
Accepted 00th January 20xx

DOI: 10.1039/x0xx00000x

www.rsc.org/

Zhiliang Wang, Miaoqiang Lyu, Peng Chen, Songcan Wang and Lianzhou Wang*

Insightful understanding of the energy loss mechanism during photoelectrochemical (PEC) process is of vital importance for efficient solar fuel production. Potential-current features under light illumination are typically used to evaluate the effectiveness of the PEC processes. However, energy loss that leads to various shapes of measured photocurrent-potential (j-E) curves is still not well understood. Herein, based on hematite photoanode, we systematically studied the photocurrent-potential-light intensity (j-E-I) relationships to acquire quantitative understanding of loss mechinsm during the PEC process by decoupling it into a photovoltaic (PV) and an electrocatalytic (EC) process. Both numerical simulation and experimental results have confired the reasonability of this analysis mehtode. It sheds light on comprehensively understanding the energy loss at semiconductor-electrolyte junction and surface electrocatalysis process for furhter optimizing PEC solar energy conversion process.

Introduction

Solar hydrogen production is one of the most promising options in achieving low-cost and sustainable production of renewable energy resources.[1-2] Photoelectrochemical (PEC) water splitting on semiconductor electrodes is highly attractive for generating solar hydrogen since it can achieve a balance of the efficiency and cost when compared with particulate photocatalysis (low cost, low efficiency) or solar cell driven electrolysis (high efficiency, high cost).[1, 3-6] Much progress has been achieved in the material development for PEC in recent years, however, the performance of PEC water splitting is still limited by serious bulk and/or surface recombination. Further optimization of this process relies on comprehensive understanding of the energy loss mechanism during the consumption of photo-generated charges.[7]

Principally, a PEC water oxidation (or reduction) involves a photo-generated holes (or electrons) consumption via electrochemical (EC) reaction at the semiconductor-electrolyte (S-E) interface where a Schottky junction is created. Due to the photovoltaic (PV) effect of the junction, photovoltage is produced to compensate the thermodynamic requirement of water oxidation. Therefore, to understand the PEC process in a system, it is necessary to deeply understand the corresponding EC and PV process.

To characterize a PEC process, photocurrent-potential (j-E) curves are usually acquired from which we can derive some important parameters, such as the onset potential (E_{onset}), saturated photocurrent (j_{sat}), and the fill factor (FF, See SI for the definition).[8] These curves can be used to identify the energy loss mechanism, including bulk recombination loss and surface reaction kinetic loss during the solar energy conversion process.[9-10] In an ideal case, the surface reaction is fast and the charge recombination in the semiconductor is negligible. Therefore, the j-E curve (type I) shows an E_{onset} approaching to the flatband potential and the j_{sat} can be predicted by Gartner equation.[11-12] It undergoes a fast increase of photocurrent at the initial potential scan, resulting in a high FF and a cross point (point i) at a high photocurrent position when combined with solar cell (j-V curve in **Scheme 1**). This type of curve can be found on InP[13] and Si[14] based photoelectrodes. Nevertheless, the most frequently observed j-E curves show an S shape (type II) with relatively large overpotential and gentle slope on electrodes such as Fe_2O_3[15], WO_3[16]. In this case, the j-V

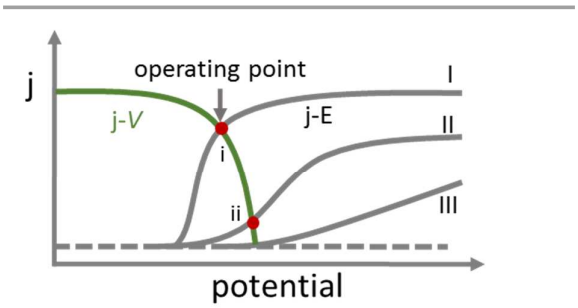

Scheme 1. The illustrated j-V curve of PV process and j-E curves of PEC process in different shapes noted as I, II and III.

Nanomaterials Centre, School of Chemical Engineering and Australian Institute for Bioengineering and Nanotechnology, The University of Queensland, QLD 4072 (Australia)
**Corresponding Author: (Lianzhou Wang). E-mail: l.wang@uq.edu.au*
Electronic Supplementary Information (ESI) available: [details of any supplementary information available should be included here]. See DOI: 10.1039/x0xx00000x

and j-E curves intersect at a point (point ii) bias from the maximum power point of the solar cell, which leads to low conversion efficiency for the un-biased water splitting.[17-18] For instance, Guruduyal et al. demonstrated that combining Fe_2O_3 with perovskite solar cell (PSC) in a tandem structure could achieve un-biased water splitting with 2.4 % STH efficiency.[19] But there is a large energy loss compared to the 10.5 % efficiency of the PSC since the operating point is not at the maximum power point of the PSC.[20] Worst of all is the type III curve, which never reaches a saturated photocurrent and the FF is very low. The high over-potential and low FF result in no intersection with the j-V curve, suggesting that it is impossible to realize un-biased reactions in such system.

In principle, the different shapes of the j-E curves are caused by different energy loss mechanism, *e.g.,* surface catalytic ability,[21] recombination centers distribution[22] and charge transfer resistance[23]. A traditional semiconductor/electrolyte model can provide some general information and understandings about the influence of these factors.[24-26] However, it fails to explain the different shapes of the j-E curves (Scheme 1) in a quantitative way, which is significant for improving the whole PEC efficiency. As comparison, the energy loss during PV or EC process has been clearly identified with suitable figure-of-merit. For example, during the PV process, the short-circuit current (j_{sc}), open-circuit potential (V_{OC}) and fill factor (FF) can reveal the charge recombination process. And for the EC process, the Tafel slope and over potential can indicate the reaction mechanism and energy barrier.

In this work, we used hematite thin film as a prototypical to investigate the light intensity dependence of some key parameters including photocurrent and photovoltage in typical PEC processes. They were used to analyse the corresponding energy loss in PV and EC process. Numerical analysis and experimental simulation are used to demonstrate how the three types of curves in Scheme 1a can be generated based on a combined PV and EC tandem system. This research is hopeful to shed light on optimizing the PEC process by reasonably analyzing the energy losing during these complicate processes.

Experiment and characterization

Fe_2O_3 photoanode fabrication

The Fe_2O_3 electrodes were prepared by a chemical bath deposition process.[15] In a typical process, the F doped SnO_2 (FTO) glass was cleaned and placed vertically in a $FeCl_3$ (0.1 M) and urea (0.15 M) aqueous solution for FeOOH deposition at 100 ^oC for 6 hours. Then the FeOOH electrode was immersed in an ethanol solution of 0.1 M titanium tetrabutoxide to achieve a Ti modification, followed by a calcination step at 600 ^oC for 3 h and 880 ^oC for 3 min to fully convert FeOOH into Fe_2O_3.

Material characterization

Morphologies of the as-prepared thin films were characterized by a field-emission scanning electron microscope (FESEM) (JSM-7100F, JEOL) and High-resolution transmission electron microscope (HRTEM) (JEM-2100, JEOL). Crystal structures of the samples were identified by a X-ray diffraction (XRD) spectroscopy (D8 Advance, Bruker) with Cu Kα (λ=0.15406 nm) radiation. UV-vis absorption spectra were obtained on a JASCOV-650 spectrophotometer.

PEC characterization

The PEC performance were measured in 1 M NaOH electrolyte (pH=13.6) in a 3-electrode system with a Pt wire as the counter electrode and a KCl saturated Ag/AgCl electrode (E^0=0.197 V_{RHE}) as the reference electrode. The potential referred to the standard reversible hydrogen electrode (RHE) is calculated according to the Nernst equation:

$$E(RHE)=E(Ag/AgCl)+0.059*pH+E^0$$

The light illumination was provided by a Xe lamp with an AM 1.5 G filter (Newport). The light intensity was controlled by a power supply as well as the working distance between the lamp and the photoelectrode. The light intensity was calibrated by a standard Si diode (Newport).A continuous change of light intensity from 0.2 Sun (20 mW cm^{-2}) to 1.9 Sun (190 mW cm^{-2}) was applied in this work.

For the linear scan voltammetry, it was recorded in the range of -0.6~0.8 V vs Ag/AgCl with a scan rate of 50 mV s^{-1}. For the photoelectrochemical impedance spectrum (PEIS), it was measured in a frequency range of 10^{-2}~10^4 Hz with an amplitude of 10 mV. When measured under constant light intensity (1 Sun, 100 mW cm^{-2}), the potential was adjusted from 0.8 to 1.3 V_{RHE}. When measured under constant potential (1.2 V_{RHE}), the light intensity was varied from 0.2 to 1.8 Sun. The PEC data was collected on an Ivium potentiostat (Ivium).

Results and discussion

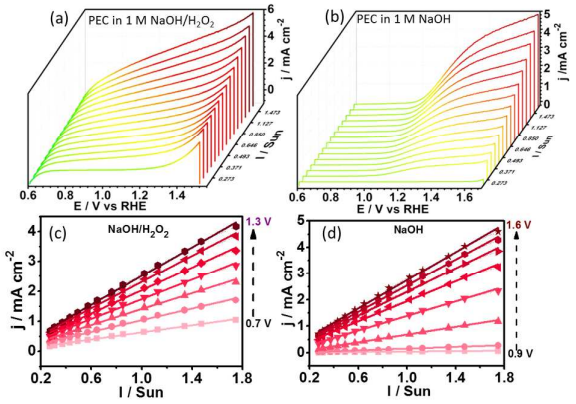

Figure 1. (a) and (b) The PEC measurements in $NaOH/H_2O_2$ and NaOH aqueous solutions with varied applied bias (E) or light intensity (I), respectively. (c) and (d) The photocurrent-light intensity relationship in $NaOH/H_2O_2$ and NaOH aqueous solution at different potentials. The adjacent j-I curves have 0.1 V potential difference.

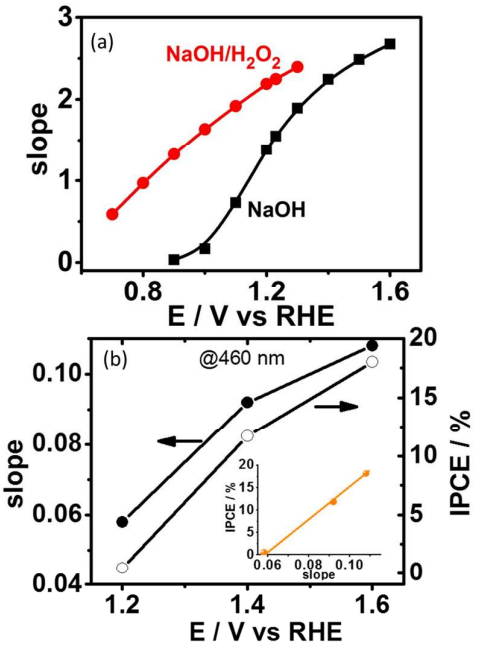

Figure 2. (a) The potential dependent slopes of j-I curves measured with (red) or without (black) H_2O_2 as scavenger. (b) The slope of j-I curves (solid dot) and IPCE (open circle) measured in NaOH aqueous solution at different potential under 460 nm illumination. The relationship between slope and IPCE is shown as insert.

The hematite thin films were prepared by a chemical bath deposition process. The XRD patterns and absorption spectra (**Figure S1**) of the thin films grown on FTO substrates confirms the formation of hematite (α-Fe_2O_3) electrode which has a bandgap about 2.0 eV. In a typical PEC measurement, the j-E curves represents the relationship between photocurrent (j) and applied potential (E) at certain light intensity (I, normally 1 Sun which is 100 mW cm^{-2} with an AM 1.5G spectrum). Actually, the photocurrent also relies on the light intensity.[26] According to the Eq. (1), we can obtain a three-dimensional (3D) pattern with varied applied biases and light intensities to reveal the j-I and E-I relationships.

$$j=f(E, I) \quad \text{(Eq. 1)}$$

Under one sun light intensity, the ideal photocurrent of the as-prepared hematite electrode is calculated to be ca. 12 mA cm^{-2} according to the absorption in Figure S1. However, the photocurrent with H_2O_2 to eliminate surface recombination was measured to be less than 4 mA cm^{-2} as shown in **Figure 1a**. It suggests that there is serious bulk recombination which leads to significant loss of the photogenerated electron-hole pairs. When further considering the surface recombination, that is photoresponse measured in NaOH without hole scavenger, the photocurrent was even lower than 3 mA cm^{-2} (**Figure 1b**). Moreover, the net photocurrent (j, current exclude the dark current. See ESI for calculation) changes linearly when varying the light intensity (I) as shown in **Figure 1 c** and **d**. In both cases, the slopes of j-I curves increase along with the improvement of applied bias. As shown in **Figure 2a**, when tested in NaOH at 1.6 V_{RHE}, the slope is about one order of magnitude larger than that at 0.8 V_{RHE}. While under the same applied potential, the presence of H_2O_2 also greatly enlarges the value of the slope.

The slope of j-I indicates how much degree the light intensity can affect the PEC process. A dimensional analysis of the unit of the slope can be expressed as follows:

$$slope \rightarrow \frac{mA/cm^2}{mW/cm^2} \rightarrow \frac{A}{W} \rightarrow \frac{n_e}{n_{ph}} \quad \text{(Eq. 2)}$$

Here n_e and n_{ph} are the amounts of consumed electrons and induced photons respectively. The ratio of n_e/n_{ph} is actually the quantum efficiency or the incident photon-to-current efficiency (IPCE) during the PEC process. Based on the results, the slope of j-I curves indicates the degree of energy loss during PEC conversion and a steeper slope means smaller loss during the photon to current conversion. Furthermore, if the photocurrent is measured under monolight illumination (λ_0), the IPCE at λ_0 should be proportional to the slopes of j-I curve. To verify it, we measured the photocurrent at different intensity at the wavelength of 460 nm (**Figure S2**). The slope of j-I curves and IPCE at varied potential are summarized in **Figure 2b**, from which a linear relationship between IPCE and slopes can be derived (insert in **Figure 2b**). This strongly suggests that the slope of j-I has a close relationship with the IPCE of the electrodes.

One-step further, based on the photocurrent recorded in NaOH and NaOH/H_2O_2, the charge injection efficiency can be calculated to evaluate the surface recombination loss [15, 27] as shown in **Figure 3**. From the nearly flat curves in **Figure 3a**, it is clear that the increase in light intensity would not affect the

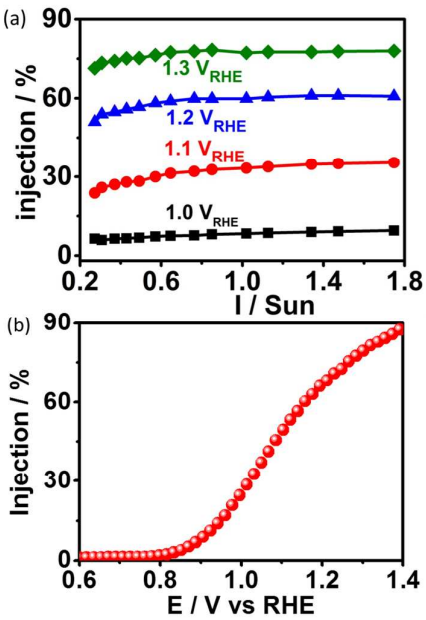

Figure 3. (a) The charge injection efficiencies under different light intensities. (b) The charge injection efficiency at different bias.

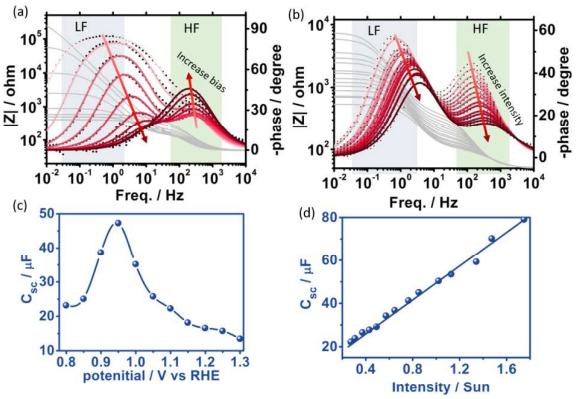

Figure 4. (a) The Bode plots of the PEIS measured under different potentials. The light intensity is 1 Sun. (b) The Bode plots of the PEIS measured under different light intensity. The potential is 1.2 V vs RHE. In (a) and (b), the red curves should refer to the left axials while the grey to the right ones. (c) and (d) The space charge layer capacity derived from (a) and (b).

surface charge injection process. Very interestingly, this behaviour is drastically different from bias dependence charge injection efficiency presented **Figure 3b**. It clearly indicates that although increasing the bias or light intensity can both lead to an improved photocurrent, the PEC process should be governed by different mechanisms in the two cases.

To better understand the promotion of PEC process via increasing bias or light intensity, we further used photoelectrochemical impedance spectra (PEIS) to analyse the charge transfer in the photoelectrodes.[28] For the PEIS measured under different potential (**Figure 4a**) or light intensity (**Figure 4b**), the Bode plots all show two peaks, suggesting at least two charge transfer processes exist during the PEC. The peak at the low frequency region is attributed to the surface reaction and the peak at high frequency region can be assigned to the charging of spacing charge layer.[29] For the low frequency peak, increasing bias or light intensity both leads to decreased peak, indicating a decreased surface reaction resistance (|Z|), that is to say, an improved surface reaction process. This is further confirmed by the increased photocurrent (**Figure 1**) and charge transfer capacitance (C_{ct}, **Figure S3**) in both cases. However, for the peaks at the high frequency, they exhibited an opposite tendency. As shown in **Figure 4c**, when improving the bias, the capacitance (C_{sc}) of space charge layer increases until the PEC water oxidation is triggered. It indicates a hole accumulation process in the space charge layer before the initiation of water oxidation.[29] After that, C_{sc} decreases fast when increasing bias. However, when increasing light intensity, the C_{sc} increases with light intensity linearly as demonstrated in **Figure 4d**.

Principally, the capacitance is defined as:

$$C = \frac{dQ}{dU} \quad \text{(Eq. 3)}$$

In the case of increased bias under constant light intensity, the amount of photogenerated charges keeps constant (dQ), so the decreased C_{SC} will lead to profound increase of built-in filed potential (dU), which provides increased driving forces for charge transfer. In the case of increase light intensity (I), since the photogenenrate charges are proportional to I, the linear relationship of C_{SC}-I in **Figure 4d** suggests a constant driving force (*dU*) during the reaction regardless of the light intensity.

In order to deeper understand the j-I relationship, we carried out a theoretical analysis about the PEC process on hematite photoelectrodes. Note that the theory about PEC on hematite should account for the experimental facts that a linear relationship of j-I and the slope represents the quantum efficiency.

Notwithstanding of the complexity of the PEC processes on the hematite, it is commonly considered that the water oxidation happens via surface states (SS).[22, 29-30] Based on Peter's model (**Figure S4**), the surface states can capture photogenerated holes and drive the Fe(III) into high valence ferrate species for H_2O oxidation (charge transfer process, Eq. 4).[30] The high valence ferrate species can also capture photogenerated electrons, resulting in the recombination of e^-/h^+ pairs (charge recombination process, Eq. 5). For hematite, the recombination process is usually non-radiative, so the energy is transferred to the vibration of the lattice, and thus the formation of phonons. These processes can be summarized as follows:[30]

Generation: $Fe_2O_3 \xrightarrow{h\nu} e^- + h^+$ (Eq. 4)

Recombination: $e^- + h^+ \xrightarrow{k_r} \text{phonon}$ (Eq. 5)

Charge transfer: $4OH^- + 4h^+ \xrightarrow{k_t} O_2 + 2H_2O$ (Eq. 6)

Where k_r and k_t are the rate constants of recombination and charge transfer, respectively.

For the charge generation process, the amount of photocharges is proportional to the absorbed light intensity. And the recombination process follows a pseudo first order rate law according to the previous work by Mi and co-workers.[3] In the charge transfer process, the reaction order, varies from 1st to 3rd order depending on the surface hole concentration.[31-32] In our case, the light intensity was varied between 0.2 to 1.9 Sun where a 1st order rate law for surface reaction is expected.[31] Therefore, the aforementioned three processes would happen at the rate shown below:

$r_g = \alpha I$ (Eq. 7)

$r_r = k_r[e^-][h^+]$ (Eq. 8)

$r_t = k_t[h^+][OH^-]$ (Eq. 9)

Where $[e^-]$ and $[h^+]$ are the surface electron and hole concentrations, $[OH^-]$ is the concentration of OH^-. During the reaction process, only very little amount of OH^- is consumed, so the $[OH^-]$ can be considered as constant. Similarly, the $[e^-]$ is also viewed as a constant for an n-type semiconductor since the intrinsic $[e^-]$ is much greater than photogenerated electrons. Under a steady-state condition, the change of surface hole density ($d[h^+]$) with the change of time (dt) is zero.[31] Thus, we can get the following equations:

$$\frac{d[h^+]}{dt} = r_g - r_r - r_t = 0 \quad \text{(Eq.10)}$$

$$r_t = \alpha \frac{K_t}{K_t + K_r} I \quad \text{(Eq. 11)}$$

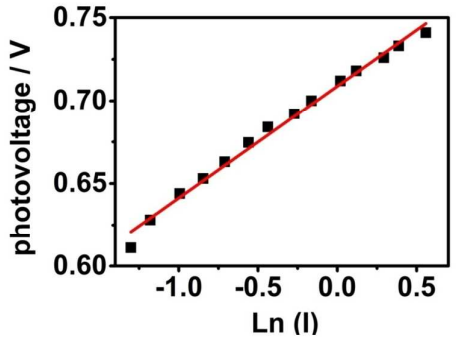

Figure 5. The relationship between light intensity and photovoltage generated at the semiconductor-electrolyte junction.

Where K_t and K_r represent $k_t[OH^-]$ and $k_r[e^-]$, respectively. The consumption of hole flux (r_t) is equivalent to the photocurrent (j). Eq. (11) suggests that the photocurrent-light intensity should have a linear relationship. As for the slope, $\alpha \frac{K_t}{K_t+K_r}$, it is actually the definition of kinetic efficiency of PEC process. Consequentially, the theoretical analysis can fit with the experimental results vide supra.

In addition to the j-I relationship, we also paid attention on the E-I relationship. In PEC process, the photovoltage provided by illumination is defined as the applied bias difference at the same current during potential scan under light and dark (**Figure S5**).[19, 33] Accordingly, the E-I relationship is replaced by the photovoltage (V)-I relationship. **Figure 5** indicates a linear relationship between photovoltage (V) and the logarithm of light intensity (*Ln I*).

Based on the discussion above, the linear relationships of j-I and V-Ln *I* strongly indicate a photovoltaic (PV) process during the PEC water oxidation process.[34-35] In general, the semiconductor/electrolyte junction can be considered as a Schottky junction to give the PV effect.[36] At the same time, the photoelectrode shows electrocatalytic ability under the dark, so we can treat the PEC as a combined PV and EC process (**Figure S6**). During the PV process, the generated photovoltage can compensate part or the total potential that inputs during the EC process, leading to a decrease of the applied bias for PEC. And the degree of voltage compensation during PEC process depends on the photocurrent. At low current, the semiconductor/electrolyte junction can generate large photovoltage, so there will be a large negative shift of potential of PEC comparing to the EC process. At high current, the generated photovoltage is low at the junction, as a result of which the j-E curves PEC come close to that of EC process.

In order to verify this assumption, we carried out a numerical simulation based on the j-V of PV and j-E of EC processes to product different type of j-E curves of PEC. For the PV process, the j-V curve is usually characterized by the short circuit current (j_{SC}), open circuit potential (V_{OC}) and fill factor (FF). For the EC process, the j-E curve is characterized by the overpotential (η), Tafel slope and the exchange current (j_0). The parameters of applied PV and EC curves in **Figure 6a** are summarized in **Table S1**. All these parameters above (i.e., j_{sc}, V_{OC}, FF for PV process and Tafel slope, η for EC process) are the key features to identify the energy loss mechanism of PV and EC process. The applied bias (E_{appl}) of PEC process is the potential difference between the EC and PV under the same current (**Figure S6, Figure 6a**). From the simulation results in **Figure 6b**, the type I j-E curves of PEC can be derived when the j-V curve of PV process has high j_{SC}, V_{OC}, FF and j-E curve of EC process has low η and slope (black lines in **Figure 6a**). While type III j-E curves can be derived when all of them are poor. For type II j-E curve, it is produced when either the PV or EC process is poor. Based on the simulation results, it is suggested that the saturated photocurrent of PEC is usually determined by PV (When the EC process is very poor, it can also limit the j_{sat}). While the E_{onset} and FF of PEC are determined by both the PV and EC process.

To further confirm the numerical simulation results of the PEC, we combined perovskite solar cells (PSCs) with different electrocatalysts, including Fe_2O_3 and NiFeP, to simulate the PV and EC process. The two PSCs show different j_{sc} and FF (**Figure 6c**): PSC-1 has higher short-circuit photocurrent and a little higher FF compared with the PSC-2. The key parameters to identify the effectiveness of PV process can be found in **Table S2**. For the EC part, NiFeP exhibits much better EC performance than Fe_2O_3 in terms of overpotential and Tafel slope (**Figure 6d, Figure S7**). After combining with PSC, the NiFeP/PSC-2 system shows a type I j-E curves with low onset

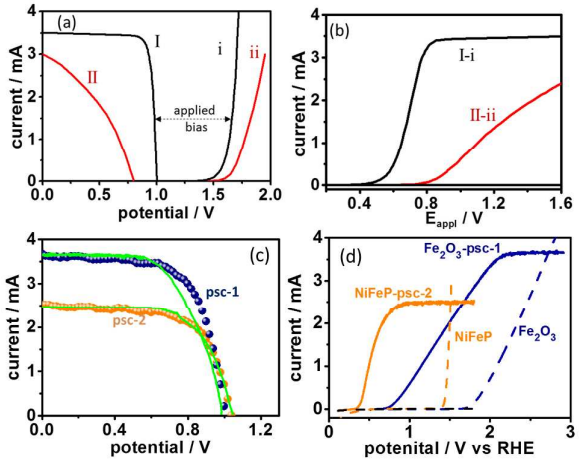

Figure 6. (a) The numeric potential-current curves of the PV (I, II) and EC (i, ii) process. (b) The numeric simulation based on the potential-current curves in (a). The I-i curve (black) is derived from I and i in (a) and II-ii curve (red) is derived from II and ii in (a). (c) The current-potential curves of two perovskite solar cells (PSCs) measured during experiment (dot) and derived from the PEC test (green line) in (d). (d) The PEC test of a simulated photoelectrode by combining the PSC with the

potential and steep current increase with the potential scan. While for the Fe_2O_3/PSC-1 system, it presents a type II curve without achieving the saturated current until a high potential. It is interesting to find that the platform photocurrent is determined mainly by the solar cell part.

According to the results above, it is reasonable to verify our hypothesis that a practical PEC system can be decoupled into a PV and an EC process. In this way, we can clarify the complex PEC process with a concise model. The energy loss mechanism of PEC can be quantitatively identified with the key parameters of EC (Tafel slope, η) and PV processes (j_{sc}, V_{OC}, FF) respectively. For the EC process, the surface reaction kinetic loss relies more on the chemical composition of the catalyst but for the photovoltaic effect, many factors can influence the performance of the solar cell. In a typical equivalent circuit of the PV process (**Figure S8**), it can be treated as an ideal current source parallel with a diode to simulate the junction. The shunt resistance (R_{sh}) is regarded to influence the fill factor of the solar cell. While the serial resistance (R_s) will influence the output potential. The R_{sh} and R_s in solar cell may come from contact resistance in solar cell.[9, 34, 37] But for PEC, they may origin from the surface states and the film resistance, respectively. So for a PEC process, a high FF can be expected if the surface states is well passivated (large R_{sh}) and the charge transfer in the electrode is excellent (low R_s). A high FF can lead to a potential high cross point (**Scheme 1**) when combined with a solar cell or other photoelectrode. For instance, after passivating the recombination states on Fe_2O_3 photoelectrode, an un-biased water splitting system with a solar-to-hydrogen (STH) efficiency of 0.91 % was achieved when combining with Pt/a-Si as photocathode.[34, 38-39]

Conclusion

In this work, we analysed the photocurrent and photovoltage dependence on light intensity to comprehensively understand the energy loss in the PEC process. The linear relationship is revealed between photocurrent and light intensity and the slope of j-I indicates the quantum efficiency of photon utilization. And the photovoltage generated in PEC process has an exponential relationship with light intensity. We then further confirmed that different PEC processes (with different shape of j-E curves) can be numerically and experimentally simulated with the PV process and EC process that have different energy loss mechanism. Accordingly, the PEC process can be simplified and the energy loss of PEC process can be well estimated via a quantitative analysis of the individual PV and EC process, which will shed light on further improving PEC system to achieve highly efficient water splitting.

Conflicts of interest

There are no conflicts to declare.

Acknowledgements

This work is supported by Australian Research Council through its DP and FF programs. The Queensland node of the Australian National Fabrication Facility is also appreciated. The authors acknowledge the facilities, and the scientific and technical assistance, of the Australian Microscopy & Microanalysis Research Facility at the Centre for Microscopy and Microanalysis, The University of Queensland.

Notes and references

1 M. G. Walter, E. L. Warren, J. R. McKone, S. W. Boettcher, Q. Mi, E. A. Santori and N. S. Lewis, *Chem. Rev.*, 2010, **110**, 6446.
2 A. J. Bard and M. A. Fox, *Acc. Chem. Res.* 1995, **28**, 141.
3 S. Chu, W. Li, Y. Yan, T. Hamann, I. Shih, D. Wang and Z. Mi, *Nano Futures*, 2017, **1,** 022001.
4 S. A. Bonke, M. Wiechen, D. R. MacFarlane and L. Spiccia, *Energy Environ. Sci.*, 2015, **8**, 2791.
5 S. Chen, T. Takata and K. Domen, *Nat. Rev. Mater.*, 2017, **2**, 201750.
6 J. R. McKone, N. S. Lewis and H. B. Gray, *Chem. Mater.*, 2013, **26**, 407.
7 K. Sivula and R. Van De Krol, *Nat. Rev. Mater.*, 2016, **1**, 15010.
8 T. Mills, F. Lin and S. W. Boettcher, *Phy. Rev. Lett.,* 2014, **112,** 148304
9 R. H. Coridan, A. C. Nielander, S. A. Francis, M. T. McDowell, V. Dix, S. M. Chatman and N. S. Lewis, *Energy Environ. Sci.*, 2015, **8**, 2886.
10 Z. Wang, Y. Qi, C. Ding, D. Fan, G. Liu, Y. Zhao and C. Li, *Chem. Sci.*, 2016, **7**, 4391.
11 H. Gerischer, in Photovoltaic and photoelectrochemical solar energy conversion, Springer, 1981, pp. 199-261.
12 P. Cendula, S. D. Tilley, S. Gimenez, J. Bisquert, M. Schmid, M. Grätzel and J. r. O. Schumacher, *J. Phy. Chem. C*, 2014, **118**, 29599.
13 L. Gao, Y. Cui, R. H. Vervuurt, D. van Dam, R. P. van Veldhoven, J. P. Hofmann, A. A. Bol, J. E. Haverkort, P. H. Notten and E. P. Bakkers, *Adv. Funct. Mater.*, 2016, **26**, 679.
14 S. Hu, M. R. Shaner, J. A. Beardslee, M. Lichterman, B. S. Brunschwig and N. S. Lewis, *Science*, 2014, **344**, 1005.
15 Z. Wang, G. Liu, C. Ding, Z. Chen, F. Zhang, J. Shi and C. Li, *J. Phy. Chem. C*, 2015, **119**, 19607.
16 J. Brillet, J.-H. Yum, M. Cornuz, T. Hisatomi, R. Solarska, J. Augustynski, M. Graetzel and K. Sivula, *Nat. Photon.*, 2012, **6**, 824.
17 S. Wang, P. Chen, Y. Bai, J. H. Yun, G. Liu and L. Wang, *Adv. Mater.*, 2018, 1800486.
18 S. H. Hsu, J. Miao, L. Zhang, J. Gao, H. Wang, H. Tao, S. F. Hung, A. Vasileff, S. Z. Qiao and B. Liu, *Adv. Mater.*, 2018, 1707261.
19 D. Sabba, M. H. Kumar, L. H. Wong, J. Barber, M. Grätzel and N. Mathews, *Nano Lett.*, 2015, **15**, 3833.
20 A. Rothschild and H. Dotan, *ACS Energy Lett.*, 2016, **2**, 45.
21 G. Liu, J. Shi, F. Zhang, Z. Chen, J. Han, C. Ding, S. Chen, Z. Wang, H. Han and C. Li, *Angew. Chem. Int. Ed.*, 2014, **53**, 7295.
22 Z. Wang, F. Fan, S. Wang, C. Ding, Y. Zhao and C. Li, *RSC Adv.*, 2016, **6**, 85582.
23 Z. Wang, X. Zong, Y. Gao, J. Han, Z. Xu, Z. Li, C. Ding, S. Wang and C. Li, *ACS Appl. Mater. Interf.*, 2017, **9,** 30696.
24 S. Soedergren, A. Hagfeldt, J. Olsson and S.-E. Lindquist, *J. Phy. Chem.*, 1994, **98**, 5552.
25 H. Gerischer, *Electrochimica Acta*, 1990, **35**, 1677.

26 D. Klotz, D. A. Grave, H. Dotan and A. Rothschild, *J. Phy. Chem. Lett.,* 2017, **8,** 1466.
27 H. Dotan, K. Sivula, M. Grätzel, A. Rothschild and S. C. Warren, *Energy Environ. Sci.*, 2011, **4**, 958.
28 L. Bertoluzzi and J. Bisquert, *J. Phy. Chem. Lett.*, 2012, **3**, 2517.
29 B. Klahr, S. Gimenez, F. Fabregat-Santiago, T. Hamann and J. Bisquert, *J. Am. Chem. Soc.*, 2012, **134**, 4294.
30 L. M. Peter, K. U. Wijayantha and A. A. Tahir, *Faraday Discuss.*, 2012, **155**, 309.
31 F. Le Formal, E. Pastor, S. D. Tilley, C. A. Mesa, S. R. Pendlebury, M. Grätzel and J. R. Durrant, *J. Am. Chem. Soc.*, 2015, **137**, 6629.
32 C. A. Mesa, A. Kafizas, L. Francàs, S. R. Pendlebury, E. Pastor, Y. Ma, F. Le Formal, M. T. Mayer, M. Grätzel and J. R. Durrant, *J. Am. Chem. Soc.*, 2017, **139**, 11537.
33 H. Dotan, N. Mathews, T. Hisatomi, M. Graetzel and A. Rothschild, *J. Phy. Chem. Lett.*, 2014, **5**, 3330.
34 J. Shi, J. Dong, S. Lv, Y. Xu, L. Zhu, J. Xiao, X. Xu, H. Wu, D. Li and Y. Luo, *Appl. Phy. Lett.*, 2014, **104**, 063901.
35 P. D. Antunez, D. M. Bishop, Y. Luo and R. Haight, *Nat. Energy*, 2017, **2**, 884.
36 R. Wilson, Critical Rev. Solid State Mater. Sci., 1980, **10**, 1.
37 R. E. Rocheleau and E. L. Miller, *Int. J. Hydrogen Energy*, 1997, **22**, 771.
38 M. T. Mayer, C. Du and D. Wang, *J. Am. Chem. Soc.*, 2012, **134**, 12406.
39 P. Yadav, M. I. Dar, N. Arora, E. A. Alharbi, F. Giordano, S. M. Zakeeruddin and M. Grätzel, *Adv. Mater.*, 2017, **29**, 1701077.